A Study of Tides, Setup and Bottom Friction in a Shallow Semi-Enclosed Basin. Part I: Field Experiment and Harmonic Analysis

J. H. FILLOUX

Scripps Institution of Oceanography, University of California at San Diego, La Jolla 92037

R. L. SNYDER

Ocean Sciences Center, Nova University, Dania, FL 33004

(Manuscript received 26 May 1976, in final form 17 July 1978)

ABSTRACT

This paper is the first in a series reporting the results of a study of tides, setup and bottom friction in the Bight of Abaco, Bahamas. The paper describes three month-long field experiments, employing 15 tide gages and four weather stations distributed throughout the Bight.

The amplitude and phase of five principal tidal constituents and the M4 and M6 overtides are estimated for all stations and errors computed from a generalization/hybridization of the algorithm of Munk and Hasselman (1964) for tidal doublets. The resulting tidal distributions constitute an unusually complete data base against which to optimize the numerical models reported in Parts II and III of the series.

The relatively small amplitude of the overtide constituents along the western margin of the Bight suggests that these constituents are locally generated. Residual fluctuations are highly coherent with the wind field. Significant differential setup effects are apparent.

1. Field experiment

Past observations of the tidal elevation of the sea surface have resulted primarily from maritime necessity. Station locations have been dictated by navigational considerations. Typically, these have clustered along coasts and inland waterways.

Recently, the development of deep sea tide gages by Snodgrass (1968), Filloux (1970) and Baker *et al.* (1973) has made tide observations possible in the deep sea. Concurrently, the development of inexpensive bottom-mounted shallow-water tide gages has simplified synoptic observations of the tide in shallower regions. Such observations are of interest because the frictional interaction is significant in such (high current) regions. Two tidal investigations using shallow-water versions of Filloux's (1970) gage have resulted. Precise cotidal and corange patterns implying unexpectedly low energy dissipation were obtained for the Gulf of California by Filloux (1973). An earlier tidal study in the Bight of Abaco, performed with exceptionally high observational coverage, is reported here.

The Bight of Abaco is a portion of the Little Bahama Bank lying between the islands of Great Abaco to the east, Little Abaco to the north, and Grand Bahama to the west. The basin is roughly 40 km × 100 km, with its major axis trending north-northwest. It is open along most of its western margin, where the bank terminates in the deep Northwest Providence Channel. Several small cays (Burrows Cay, Mores Island, Gorda Cay) mark this edge of the bank. A secondary opening to the northwest between Little Abaco and Grand Bahama connects the Bight with the main portion of the Little Bahama Bank to the north and east of Grand Bahama.

The geometry and bottom topography of the region is shown in Fig. 1. The soundings in this figure, obtained primarily from surveys conducted during the field experiment, differ somewhat from those reported in Hydrographic Charts of the area. The main features of the bottom topography are the broad 9 m depression lying in the northern half of the basin, the 2–5 m sill along the western opening (marked by numerous 1–3 m sand bores), the broad 4 m flat lying in the southern third of the basin, and the extensive area of small islands, shallow channels and mangroves (The Marls) to the east.

The region is sufficiently shallow that, despite its small size, semidiurnal phase differences as large as 120° are developed within its borders. The tidal topography is accordingly neither trivial nor overly complex, and is thus a reasonable focus for the numerical model to be presented in Part II. Furthermore, measurable overtides are present; as will be seen in Part II, these result from nonlinear interactions within the Bight (in part from bottom fric-

0022-3670/79/010158-12$07.00

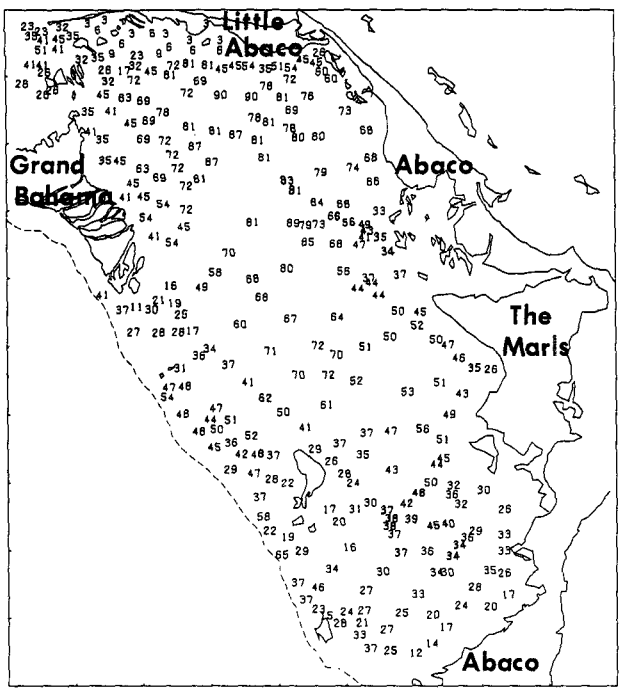

FIG. 1. Geography and bottom topography of the Bight of Abaco, Bahamas. Soundings (decimeters below mean sea level) are based on private surveys and an 1884 survey of the Hydrographic Office. The dotted line is essentially the 200 m (100 fathom) contour. The Marls is a region of small islands and mangroves. Scale is 10 km per division.

tion interactions). The strong depth discontinuity along the western opening simplifies the formulation of an appropriate boundary condition for these overtide constituents. These features also work to the advantage of the numerical model.

To provide data against which to optimize this model, we conducted a series of three month-long field experiments in 1969–70. The first of these took place during February–March 1969, the second during July–August 1969, and the third during July–August 1970. During each experiment, 15 shallow-water Filloux gages and four weather stations (similar gages adapted to measure atmospheric pressure, wind speed and wind direction) were deployed in the configurations shown in Fig. 2. Each tide gage was placed on the bottom, attached to a 100 m polyethylene tagline and marked by a nearby surface float, as shown in Fig. 3. Recovery of the gage was accomplished by dragging a small grapnel across the tagline. Instrument positions were determined with Decca Hi-Fix using various baselines (Miami-

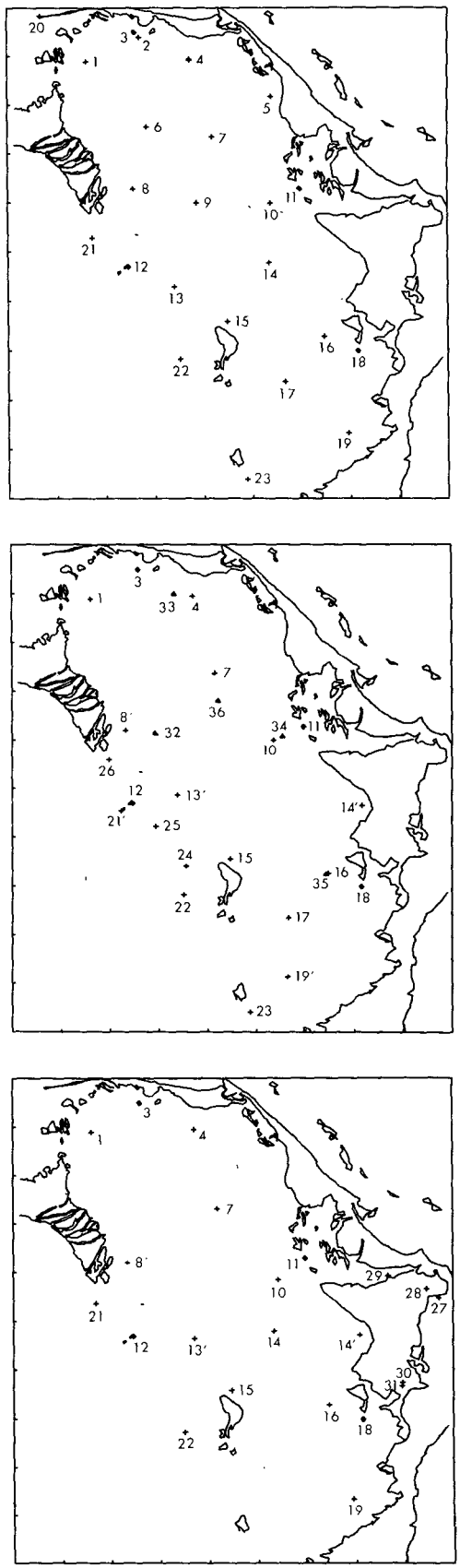

FIG. 2. Instrument configurations for the (1) February–March 1969, (2) July–August 1969 and (3) July–August 1970 experiments. Stations 3, 11, 12 and 18 (◇) are land-based weather stations; the remaining stations (+) are bottom-mounted tide gages. A reed switch gage was deployed at Station 4 (experimental site).

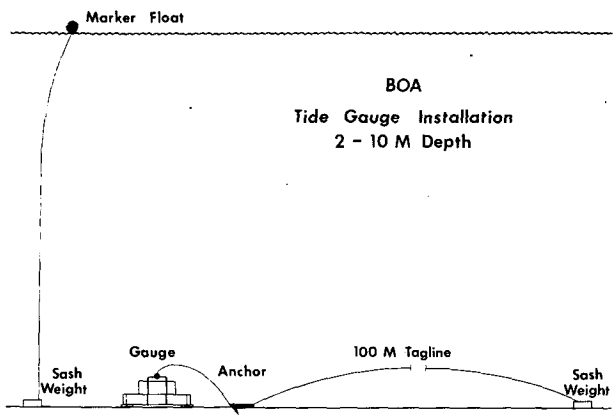

FIG. 3. Installation of the bottom-mounted tide gages.

Jupiter Inlet for the February–March 1969 experiment, Allan's Pensacola Cay-Hopetown for the July–August 1969 experiment, and Miami-Fort Lauderdale for the July–August 1970 experiment). Despite the loss of a number of marker floats, recovery of the gages was 100% successful, with over 90% yielding usable data.

Additional data were provided by a reed switch tide gage built by D. G. Hunley (unpublished). This instrument has a range of 1.5 m and a step size of 0.6 cm; data are acquired photographically. It was deployed at Station 4 during each field experiment and also from 28 December 1969 to 15 May 1970, and from 21 May 1970 to 9 August 1970. It was deployed midway between Stations 8 and 13 from 27 October 1971 to 2 November 1971. The reed switch tide gage measures the surface elevation ζ directly. The bottom-mounted tide gages measure $\zeta + (1/\rho g)p$, where p is the atmospheric pressure, ρ the density (assumed constant) and g the acceleration of gravity. A comparison of the two gages is provided by the Station 4 records during the February–March 1969 experiment. Using Station 3 atmospheric pressure to adjust the bottom-mounted tide gage record, the difference between the tide records was computed. The root mean square difference was 1.9 cm; the maximum difference was 6.3 cm. These may be compared with resolutions of 0.6 cm for the reed switch gage and 1 cm for the bottom-mounted gage. A tidal analysis of the difference signal suggests that the variance is only 10% tidal. Cross-spectral analysis with the mean wind speed at Station 3 indicates that this difference is largely incoherent with wind speed. Because the spectrum of the difference is distinctly red in character, we speculate that this difference is largely temperature-induced.

The weather station barographs were packed in vermiculite and buried under 0.3 m of sand. A nearby 3 m mast supported a Taylor anemometer and vane. The three signals were acquired simultaneously on a single Rustrak recorder inside the barograph.

The tide gage data from the three field experiments are displayed in the Appendix. Several features are immediately evident:

1) The amplitude of the tide inside the Bight is considerably smaller than it is along the western opening. Inside the Marls region, this amplitude is further drastically reduced.

2) The tide is largely semidiurnal in character.

3) Non-tidal fluctuations are apparent in all three field experiments, particularly in the February–March 1969 experiment.

The weather station data from the three field experiments are also shown in the Appendix. We note the following features:

1) The weather pattern for the February–March experiment differs considerably from those for the two summer experiments.

2) The February–March experiment is characterized by a succession of frontal passages (during one 10-day section of record, four distinct fronts passed through the area), during which the wind direction veered rapidly from southwest to northwest, settling in the northwest-north for periods of 1–5 days with fresh winds of 8–14 m s^{-1}.

3) The summer experiments were characterized by relatively stable conditions with the winds typically east to southwest at speeds of 1–8 m s^{-1}.

4) The weather data for a given experiment are highly coherent from station to station.

2. Analytical approach

The data presented in the previous section contain contributions from several classes of motions (principally tidal motions and setup motions). Other motions contribute to Bight dynamics but are excluded from the data by the bandpass characteristics of the instrumentation (steady motions, surface wave motions and turbulence). Because the system is nonlinear, these various motions are coupled, a serious dynamical complication but also an important focal point for the subsequent analysis.

The typical tide/setup model computation avoids this complication by treating composite motions. In modeling the Bight of Abaco data in Parts II and III of this series, we have chosen rather to deal with each component of the motion separately, treating the nonlinear coupling from other components as given, and imagining that we can sequentially iterate all component computations until a convergent result is obtained. In so doing we believe that we render the physics of the system more transparent.

Separation of the tidal and setup motions is dif-

ficult because the scales of these motions are not distinct. Furthermore, because the meteorology is in part tidally forced, certain motions, i.e., tidally induced setup motions, cannot be unambiguously classified. Therefore, any prescription for separating these motions is clearly somewhat arbitrary. To effect a separation we choose to exploit a salient characteristic of all tidal fluctuations, namely, their almost periodic character. Accordingly, we identify the almost periodic component of the motion as the tidal component and the long-period nonperiodic residual as the "setup" component. (Using this prescription, tidally induced setup motions are tidal in character.)

In the next section we follow this prescription to separate the experimental data, using a least-squares harmonic analysis to estimate the tidal component of the data. In the final section we estimate the corresponding residual setup. We also estimate the errors in both computations, viewing the setup component as a random variable.

In Parts II and III of the series we effect a corresponding separation of the dynamical equations, developing numerical models to solve for the tidal (and tidally averaged) setup components of the motion, respectively. A crucial aspect of these models is the representation of the bottom friction term coupling the motions.

3. Harmonic analysis

In keeping with the remarks of the previous section, the long-period component of the surface elevation (periods >1 h) is taken to be of the form

$$\zeta = \zeta_H + \zeta_R,$$

with

$$\zeta_H \equiv \frac{1}{2} \sum_{n=-\infty}^{\infty} {}_n\zeta_H H_n,$$

$$H_n(t) \equiv \exp[i(\omega_n t + \Phi_n].$$

Here $\zeta(\mathbf{x},t)$ is the surface elevation at horizontal position $\mathbf{x}$ and time t, $\zeta_H(\mathbf{x},t)$ is the tidal component of this elevation, and $\zeta_R(\mathbf{x},t)$ is the residual "setup" fluctuation. ${}_n\zeta_H(\mathbf{x})$ is the (complex) amplitude for the tidal constituent with frequency ω_n. ${}_n\zeta_H$, ω_n and Φ_n satisfy the relations ${}_{-n}\zeta_H(\mathbf{x}) = {}_n\zeta_H(\mathbf{x})^*$, $\omega_{-n} = -\omega_n$ and $\Phi_{-n} = -\Phi_n$. The tidal frequencies ω_n are integral linear combinations of the frequencies $\Omega_1 \approx 2\pi/1.035$ days, $\Omega_2 \approx 2\pi/27.32$ days, $\Omega_3 \approx 2\pi/$year, $\Omega_4 \approx 2\pi/8.847$ years, $\Omega_5 \approx 2\pi/18.61$ years, and $\Omega_6 \approx 2\pi/20940$ years, defined by the celestial mechanics of the earth-moon-sun system. Φ_n is the phase of the corresponding constituent of the equilibrium tide at Greenwich evaluated at time zero (principal constituents). This formulation implies that the phase of ${}_n\zeta_H(\mathbf{x})$ is the phase of the constituent relative to the equilibrium tide at Greenwich.

Given an indefinitely long record, the amplitudes ${}_n\zeta_H(\mathbf{x})$ and the residual fluctuation $\zeta_R(\mathbf{x},t)$ can in principle be determined exactly. In practice, the finite length of tidal records and the residual noise present in these records, imply that only a finite number N of complex amplitudes ${}_n\zeta_H$ can be estimated, and that the corresponding estimates are subject to an error dependent on the frequency set, the length of record and the spectrum of the residual fluctuation. Munk and Hasselmann (1964) analytically calculate this error for a pair of closely spaced tidal constituents. Numerically the error depends on the scalar product matrix (defined by the least-squares problem) and its inverse. We let (ψ,χ) be the scalar product of the real variables $\psi(t)$ and $\chi(t)$, i.e.,

$$(\psi,\chi) \equiv \int_{t_0}^{t_0+T} dt\,\psi\chi,$$

where T is the record length. For given $\mathbf{x}$, we demand that the norm (self-scalar product) of the (estimated) residual

$$\zeta_R' \equiv \zeta - \frac{1}{2} \sum_{n=-N}^{N} {}_n\zeta_H' H_n$$

be a minimum with respect to the (estimated) complex amplitudes ${}_n\zeta_H'$, subject to the auxiliary conditions

$${}_{-n}\zeta_H' = {}_n\zeta_H'^*.$$

This demand may be formulated in such a way as to involve only real variables without auxiliary conditions by making the transformation

$$I_{2n-1} \equiv \mathrm{Re}H_n = \frac{1}{2}(H_n + H_{-n}) = \cos(\omega_n t + \Phi_n),$$

$$I_{2n} \equiv \mathrm{Im}H_n = \frac{1}{2i}(H_n - H_{-n}) = \sin(\omega_n t + \Phi_n),$$

$${}_{2n-1}\zeta_I \equiv \mathrm{Re}\ {}_n\zeta_H = \frac{1}{2}({}_n\zeta_H + {}_{-n}\zeta_H),$$

$${}_{2n}\zeta_I \equiv -\mathrm{Im}\ {}_n\zeta_H = -\frac{1}{2i}({}_n\zeta_H - {}_{-n}\zeta_H),$$

$$n = 1, 2, \cdots, N,$$

so that

$$\zeta_H = \zeta_I \equiv \sum_{n=1}^{\infty} {}_n\zeta_I I_n,$$

$$\zeta_R' = \zeta - \sum_{n=1}^{2N} {}_n\zeta_I' I_n.$$

Differentiating with respect to the ${}_n\zeta_I'$'s, we obtain the $2N$ conditions

$$\sum_{m=1}^{2N} (I_n,I_m)_m\zeta_I' = (I_n,\zeta), \quad n = 1, 2, \cdots, 2N,$$

which may be inverted to give

$$ {}_m\zeta_I' = \sum_{n=1}^{2N} {}_{mn}S_I^{-1}(I_n,\zeta), $$

where ${}_{nm}S_I \equiv (I_n,I_m)$, and S_I^{-1} is an inverse to S_I of order $2N$. It follows that

$$ {}_m\zeta_I' = {}_m\zeta_I + \sum_{l=2N+1}^{\infty} {}_{ml}E_I\ {}_l\zeta_I + \sum_{n=1}^{2N} {}_{mn}S_I^{-1}(I_n,\zeta_R), \quad (1) $$

where

$$ {}_{ml}E_I \equiv \sum_{n=1}^{N} {}_{mn}S_I^{-1}\ {}_{nl}S_I. $$

The second and third terms on the right represent errors resulting from tidal constituents not included in the analysis and from the residual fluctuations, respectively. In principle, the former can be reduced by including a sufficient number of constituents in the analysis; however, the additional constituents adversely affect the errors associated with the latter. The third term is the term dealt with by Munk and Hasselmann. To see this relationship, we introduce a statistical description of the residual fluctuation $\zeta_R(\mathbf{x},t)$ where angle braces denote the corresponding ensemble average. We assume

$$ \langle \zeta_R \rangle = 0, $$

so that

$$ \langle \zeta \rangle = \zeta_H = \zeta_I. $$

Also,

$$ \langle {}_n\zeta_I' \rangle = {}_m\zeta_I + \sum_{l=2N+1}^{\infty} {}_{ml}E_I\ {}_l\zeta_I, $$

$$ \langle {}_n\zeta_I'\ {}_m\zeta_I' \rangle - \langle {}_n\zeta_I' \rangle \langle {}_m\zeta_I' \rangle = \sum_{p=1}^{2N}\sum_{q=1}^{2N} {}_{np}S_I^{-1}\ {}_{mq}S_I^{-1} \langle (I_p,\zeta_R)(I_q,\zeta_R) \rangle. $$

Precise evaluation of the bracketed term is a task of some algebraic complexity. This task is simplified if ζ_R is quasi-stationary and if T is very large compared with the correlation time of the residual fluctuation ζ_R. In this case,

$$ \langle (I_p,\zeta_R)(I_q,\zeta_R) \rangle = \int_{t_0}^{t_0+T} dt \int_{t_0-t}^{t_0+T-t} d\tau I_p(t) I_q(t+\tau) C_{\zeta_R^2}(t,\tau) $$

$$ \approx \int_{t_0}^{t_0+T} dt \int_{-\infty}^{\infty} d\tau I_p(t) I_q(t+\tau) C_{\zeta_R^2}(t,\tau), $$

where

$$ C_{\zeta_R^2}(t,\tau) = \langle \zeta_R(\mathbf{x},t)\zeta_R(\mathbf{x}, t+\tau) \rangle. $$

For $I_p(t) = \cos(\omega_p t + \Phi_p)$ and $I_q(t) = \cos(\omega_q t + \Phi_q)$, this integral takes the form

$$ \langle (I_p,\zeta_R)(I_q,\zeta_R) \rangle \approx 2\pi \int_{t_0}^{t_0+T} dt \cos(\omega_p t + \Phi_p) \cos(\omega_q t + \Phi_q) E_{\zeta_R^2}(t,\omega_q), $$

where

$$ E_{\zeta_R^2}(t,\omega) \equiv \frac{1}{2\pi} \int_{-\infty}^{\infty} d\tau C_{\zeta_R^2}(t,\tau) \cos\omega\tau $$

is the (two-sided) spectrum of ζ_R. (Since $C_{\zeta_R^2}$ is

TABLE 1. Harmonic analysis of selected tide and atmospheric pressure records showing the amplitudes (cm) and phase lags (deg) relative to equilibrium tide at Greenwich. Standard deviations are computed from relations (4) and (5). Tidal constants are uncorrected for atmospheric pressure. t_0 is the start time in days from 0000 GMT 1 January 1968, T the record length in days.

STN	t_0	T	O1		K1		N2		M2		S2		M4		M6	
TIDE RECORDS																
20	437.8	6.7	8.0±1.9	235.±14.	7.4±2.1	228.±17.	5.8±5.5	24.±54.	22.5±7.4	50.±18.	7.3±3.0	73.±24.	0.5±0.2	352.±25.	1.0±0.2	189.±10.
1	405.7	38.1	5.4±0.3	266.±3.	5.2±0.3	270.±4.	2.7±0.3	84.±7.	18.8±0.3	111.±1.	3.6±0.3	143.±5.	0.9±0.1	162.±7.	0.7±0.1	30.±6.
1	558.9	28.7	5.3±0.3	269.±3.	6.4±0.3	292.±2.	4.3±0.3	98.±4.	19.2±0.3	122.±1.	2.3±0.3	169.±8.	0.7±0.1	181.±10.	0.5±0.1	53.±11.
1	930.5	11.3	5.4±0.4	278.±4.	6.3±0.4	287.±4.	3.6±1.0	115.±17.	18.9±1.1	125.±3.	2.2±0.6	129.±15.	1.0±0.1	188.±7.	0.7±0.1	75.±10.
2	405.9	31.8	5.4±0.4	268.±4.	5.1±0.4	276.±4.	2.3±0.3	89.±7.	18.1±0.3	120.±1.	3.5±0.3	155.±5.	0.9±0.1	175.±7.	0.5±0.1	36.±8.
10	407.6	31.1	5.1±0.4	264.±5.	5.7±0.4	267.±4.	2.2±0.2	63.±6.	14.5±0.2	97.±1.	2.8±0.2	116.±5.	0.5±0.1	109.±16.	0.7±0.1	297.±9.
10	561.7	30.0	4.9±0.2	261.±3.	5.6±0.2	274.±2.	3.8±0.2	68.±4.	15.9±0.2	97.±1.	2.6±0.2	131.±5.	0.5±0.1	123.±10.	0.7±0.1	284.±7.
10	922.6	27.8	5.2±0.3	265.±3.	5.6±0.3	273.±3.	3.4±0.3	85.±5.	15.4±0.3	96.±1.	2.7±0.3	133.±6.	0.5±0.1	112.±10.	0.7±0.1	292.±7.
15	409.6	30.6	4.7±0.3	249.±4	5.7±0.3	261.±3.	2.7±0.3	29.±6.	13.4±0.3	57.±1.	4.0±0.3	83.±4.	0.7±0.1	62.±11.	0.7±0.1	225.±8.
15	565.0	27.7	4.9±0.2	243.±3.	5.7±0.2	258.±3.	3.8±0.2	33.±4.	15.6±0.2	60.±1.	3.1±0.2	98.±5.	0.9±0.1	75.±8.	0.8±0.1	226.±7.
15	921.6	32.4	4.6±0.2	242.±3.	5.5±0.2	252.±2.	3.4±0.3	47.±4.	14.8±0.3	60.±1.	3.0±0.2	111.±5.	1.1±0.1	96.±7.	0.7±0.1	217.±8.
19	409.9	38.9	5.0±0.6	246.±7.	6.4±0.6	259.±6.	3.7±0.6	46.±9.	19.6±0.6	60.±2.	5.6±0.5	90.±5.	2.1±0.3	80.±7.	0.1±0.1	9.±83.
21	920.6	31.0	7.8±0.3	210.±2.	9.1±0.3	215.±2.	10.0±0.6	10.±4.	39.4±0.6	14.±1.	6.8±0.6	60.±5.	0.3±0.1	117.±18.	0.2±0.1	281.±27.
22	920.8	33.7	7.3±0.4	203.±3.	9.6±0.4	210.±2.	9.6±0.4	355.±2.	37.4±0.4	10.±1.	6.3±0.4	62.±4.	0.3±0.1	99.±16.	0.2±0.1	272.±16.
23	562.9	30.7	7.3±0.4	201.±3.	10.0±0.4	211.±2.	9.7±0.6	341.±4.	39.2±0.6	6.±1.	6.7±0.6	56.±5.	0.2±0.1	118.±28.	0.3±0.1	229.±12.
ATMOSPHERIC PRESSURE RECORDS																
3	921.9	30.7	0.2±0.1	73.±38.	0.5±0.1	130.±11.	0.1±0.1	58.±41.	0.0±0.1	205.±107.	0.8±0.1	107.±5.	0.0±0.0	200.±60.	0.0±0.0	317.±57.
11	410.8	35.0	0.1±0.2	77.±91.	0.5±0.2	341.±19.	0.0±0.1	27.±90.	0.1±0.1	69.±48.	1.0±0.1	87.±4.	0.0±0.0	277.±57.	0.0±0.0	128.±52.
11	557.1	31.4	0.0±0.1	105.±168.	0.4±0.1	117.±16.	0.0±0.1	95.±123.	0.1±0.1	173.±28.	0.9±0.0	93.±3.	0.0±0.0	22.±39.	0.0±0.0	208.±50.
11	920.7	31.0	0.2±0.1	91.±24.	0.9±0.1	102.±7.	0.1±0.1	39.±59.	0.1±0.1	244.±55.	0.8±0.1	112.±4.	0.0±0.0	115.±85.	0.0±0.0	107.±346.
12	924.7	30.2	0.2±0.1	97.±37.	0.7±0.1	130.±11.	0.1±0.1	24.±54.	0.0±0.1	271.±74.	0.7±0.1	105.±4.	0.0±0.0	193.±60.	0.0±0.0	110.±63.
18	923.8	30.0	0.1±0.1	108.±63.	0.4±0.1	119.±14.	0.1±0.1	66.±58.	0.0±0.1	326.±117.	0.7±0.1	106.±4.	0.0±0.0	58.±83.	0.0±0.0	347.±91.

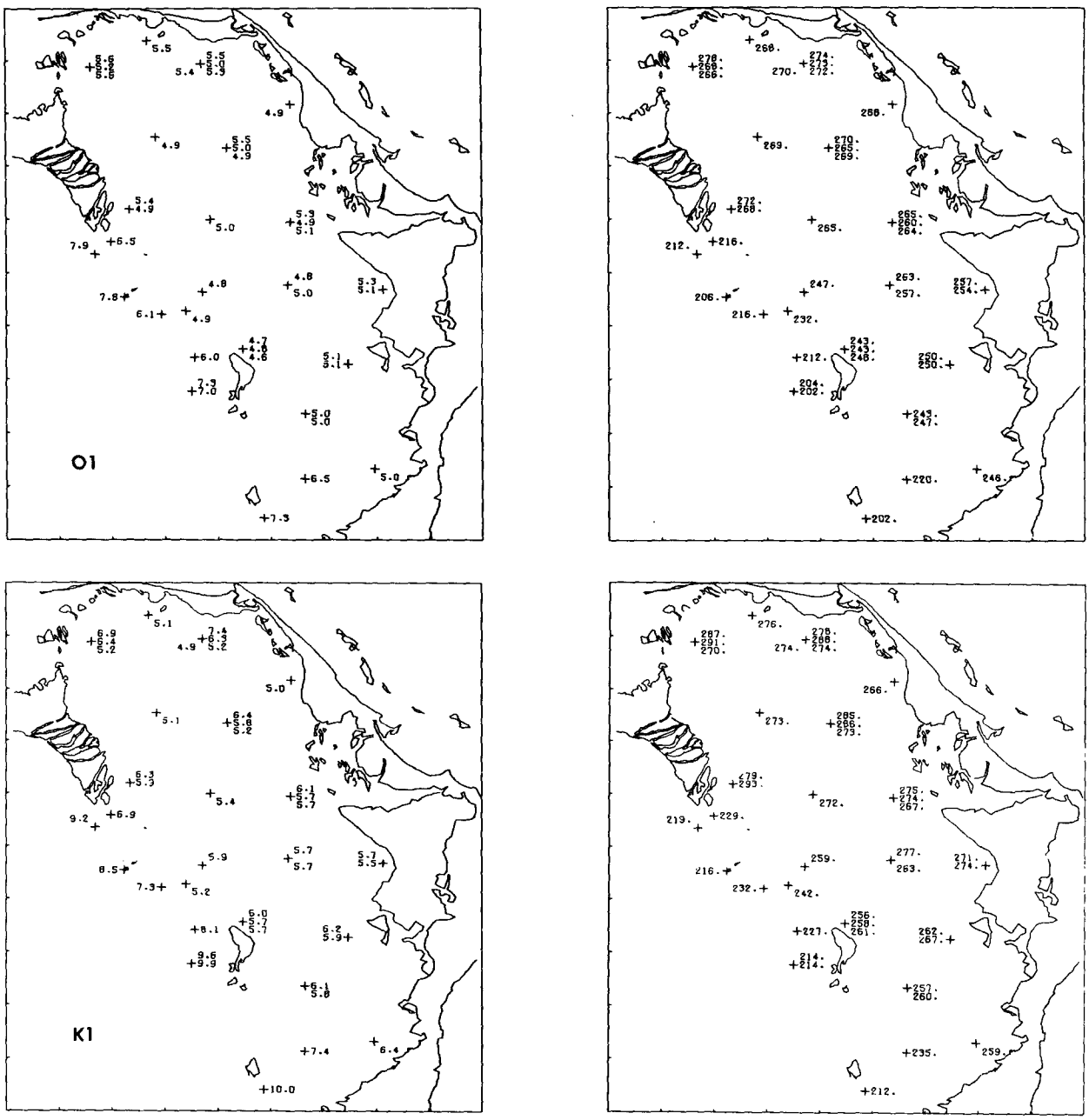

FIG. 4. Amplitude and phase of the diurnal constituents, O1 and K1. Left-hand panels show amplitude (cm); right-hand panels show phase lag (deg) relative to equilibrium tide at Greenwich.

approximately an even function of τ, the corresponding sine integral is approximately zero.) For $\omega_p = \omega_q$, the leading term in the integral is of order T^1, i.e.,

$$\langle (I_p,\zeta_R)(I_p,\zeta_R)\rangle \approx \pi T E_{\zeta_R^2}(\bar{t},\omega_p) + O(T^0),$$

where from the mean value theorem, $\bar{t}$ is some t in the interval

$$t_0 < \bar{t} < t_0 + T.$$

Similarly, for $\omega_p \neq \omega_q$,

$$\langle (I_p,\zeta_R)(I_q,\zeta_R)\rangle \approx O(T^0).$$

Likewise, for $I_p(t) = \sin(\omega_p t + \Phi_p)$ and $I_q(t) = \sin(\omega_q t + \Phi_q)$,

$$\langle (I_p,\zeta_R)(I_q,\zeta_R)\rangle \approx \pi T E_{\zeta_R^2}(\bar{t},\omega_p) + O(T^0), \quad \omega_p = \omega_q,$$
$$\approx O(T^0), \quad \omega_p \neq \omega_q.$$

Finally, for $I_p(t) = \cos(\omega_p t + \Phi_p)$ and $I_q(t) = \sin(\omega_q t + \Phi_q)$ or for $I_p(t) = \sin(\omega_p t + \Phi_p)$ and $I_q(t) = \cos(\omega_q t + \Phi_q)$,

$$\langle (I_p,\zeta_R)(I_q,\zeta_R)\rangle \approx O(T^0).$$

In general,

$$\langle (I_p,\zeta_R)(I_q,\zeta_R)\rangle \approx \delta_{pq}\pi T E_{\zeta_R^2}(\bar{t},\omega_p) + O(T^0),$$

where δ_{pq} is the Kronecker delta. It follows that

$$\langle {}_n\zeta_I' \, {}_m\zeta_I'\rangle - \langle {}_n\zeta_I'\rangle\langle {}_m\zeta_I'\rangle \approx \pi T \sum_{p=1}^{2N} {}_{np}S_I^{-1} \, {}_{mp}S_I^{-1} E_{\zeta_R^2}(\bar{t},\omega_p) + O(T^0). \quad (2)$$

This result is a generalization of and hybridization of the Munk-Hasselmann (1964) relation. The factor of $E_{\zeta_R^2}$ is explicit; the $\Delta\omega$ dependence of the Munk-Hasselmann relation is implicit in the numerically calculated inverse matrix S_I^{-1}. The relation as derived here lends itself naturally to a numerical evaluation of the covariance matrix

$$\langle {}_n\zeta_I' \, {}_m\zeta_I'\rangle - \langle {}_n\zeta_I'\rangle\langle {}_m\zeta_I'\rangle$$

as an integral feature of the harmonic analysis.

As a matter of practical analysis, the summation contained in relation (2) need typically be carried out only over terms belonging to the same species of tidal constituents. Thus

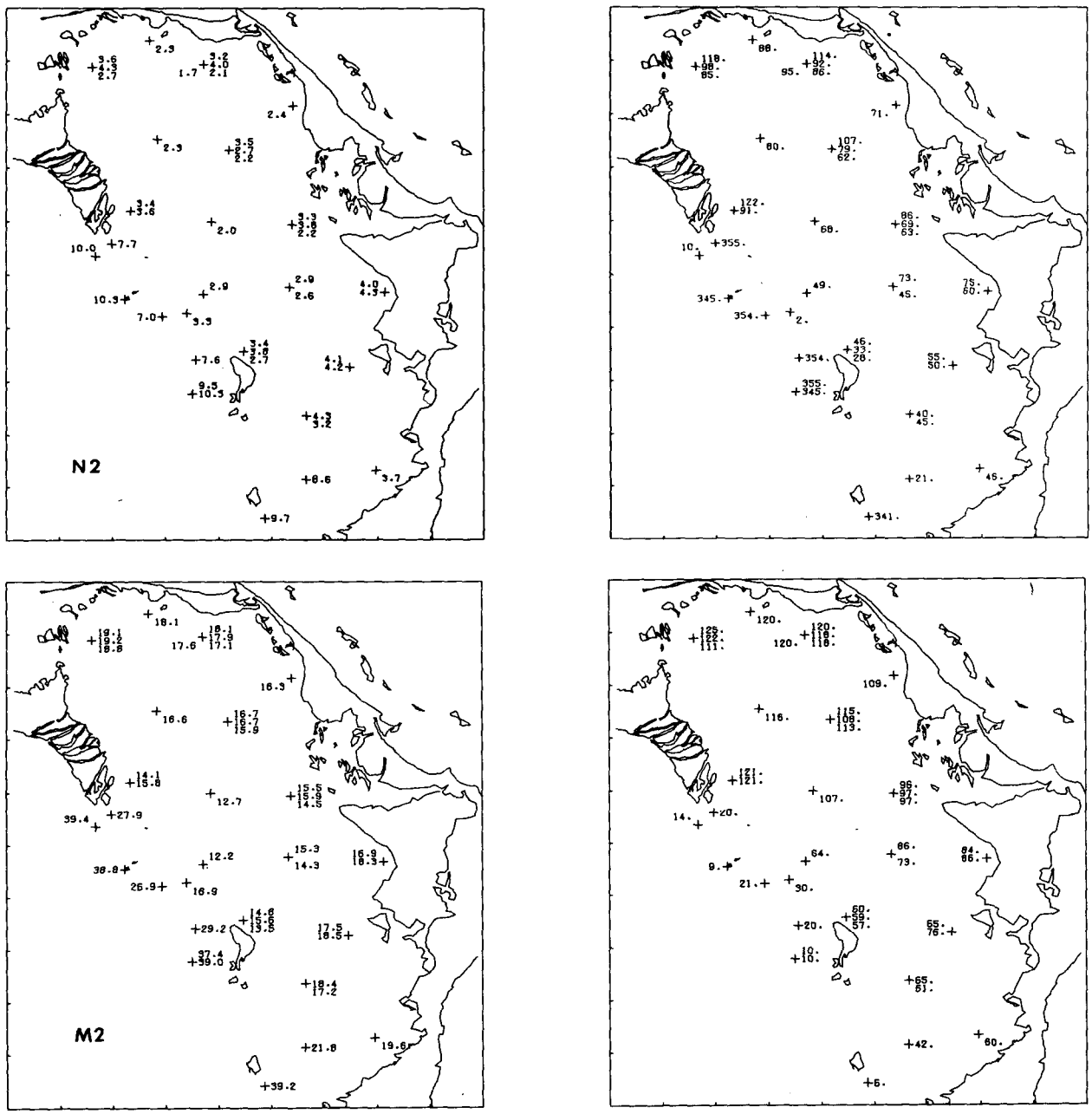

FIG. 5. As in Fig. 4 except for the semi-diurnal constituents N2, M2 and S2.

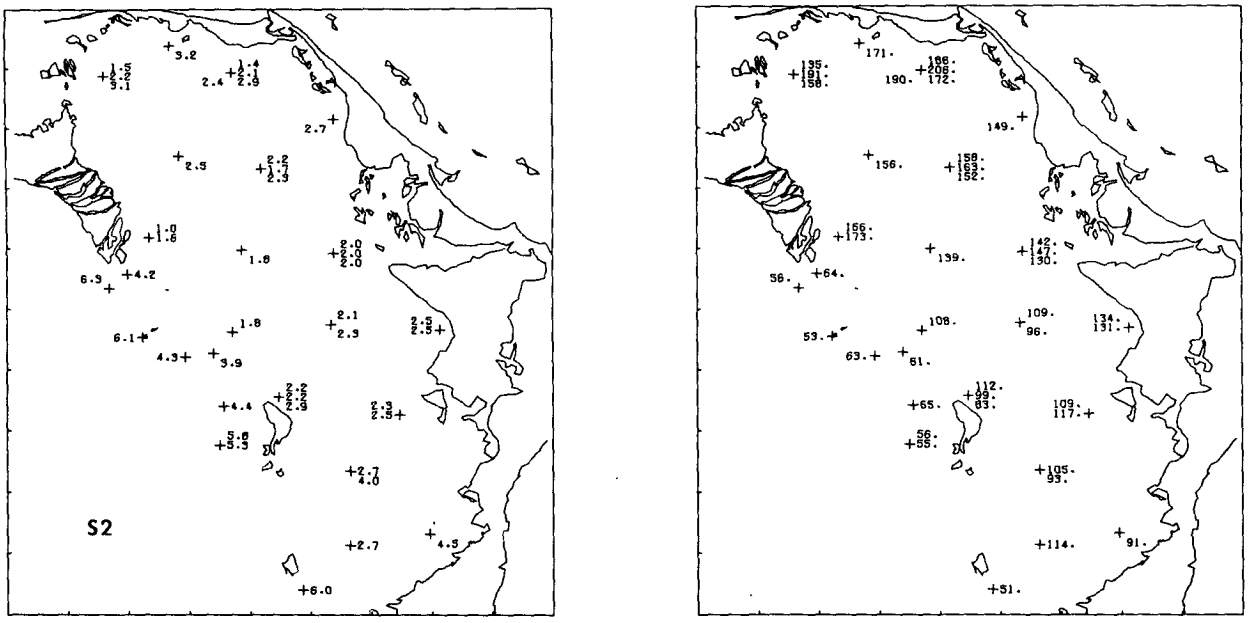

FIG. 5. (*Continued*)

$$\langle {}_n\zeta_I' \, {}_m\zeta_I' \rangle - \langle {}_n\zeta_I' \rangle \langle {}_m\zeta_I' \rangle$$

$$\approx \pi T E_{\zeta_R^2}(\bar{t},\Omega_0) \sum_p {}_{np}S_I^{-1} \, {}_{mp}S_I^{-1}, \quad m, n \text{ diurnal,}$$

diurnal constituents

$$\approx \pi T E_{\zeta_R^2}(\bar{t},2\Omega_0) \sum_p {}_{np}S_I^{-1} \, {}_{mp}S_I^{-1}, \; m, n \text{ semidiurnal,}$$

semidiurnal constituents

$$\approx 0, \; m, \; n \text{ mixed diurnal, semidiurnal,} \qquad (3)$$

where $\Omega_0 \equiv 2\pi/\text{day}$.

An harmonic analysis of the BOA data was performed for the constituents O1, K1, N2, M2, S2, M4 and M6, with reference phases for the overtide constituents M4 and M6 defined as suitable multiples of the reference phase for M2. A summary of this analysis is given in Table 1 for selected tide and atmospheric pressure records. Amplitude and phase errors were calculated from the corresponding covariances (3), i.e., if

$${}_n\Phi_H' \equiv -\arg {}_n\zeta_H' = -\tan^{-1}({}_{2n-1}\zeta_I'/{}_{2n}\zeta_I'),$$

$$|{}_n\zeta_H'| \equiv \text{mod } {}_n\zeta_H' = ({}_{2n-1}\zeta_I'^2 + {}_{2n}\zeta_I'^2)^{1/2},$$

and if $V(\Psi,\chi)$ denotes the covariance

$$V(\psi,\chi) \equiv \langle \Psi\chi \rangle - \langle \Psi \rangle \langle \chi \rangle,$$

then

$$|{}_n\zeta_H'|^2 V(|{}_n\zeta_H'|, |{}_n\zeta_H'|) = {}_{2n-1}\zeta_I'^2 V({}_{2n-1}\zeta_I', {}_{2n-1}\zeta_I') + 2 \, {}_{2n-1}\zeta_I' \, {}_{2n}\zeta_I' V({}_{2n-1}\zeta_I', {}_{2n}\zeta_I') + {}_{2n}\zeta_I'^2 V({}_{2n}\zeta_I', {}_{2n}\zeta_I'), \qquad (4)$$

$$|{}_n\zeta_H'|^4 V({}_n\Phi_H', {}_n\Phi_H') = {}_{2n-1}\zeta_I'^2 V({}_{2n-1}\zeta_I', {}_{2n-1}\zeta_I') - 2 \, {}_{2n-1}\zeta_I' \, {}_{2n}\zeta_I' V({}_{2n-1}\zeta_I', {}_{2n}\zeta_I') + {}_{2n}\zeta_I'^2 V({}_{2n}\zeta_I', {}_{2n}\zeta_I'). \qquad (5)$$

The errors shown are $V(|{}_n\zeta_H'|, \; |{}_n\zeta_H'|)^{1/2}$ and $V({}_n\Phi_H', {}_n\Phi_H')^{1/2}$.

Examination of Table 1 shows the following:

1) Estimates of the amplitude and phase of a given constituent at a given station are not generally consistent within the computed statistical errors. The lack of better agreement is probably the result of the second term on the right-hand side of (1), resulting from the presence of other tidal constituents not included in the analysis.

2) The shorter records do not permit an accurate determination of the amplitude and phase of all seven constituents analyzed (the errors are large).

3) Phase differences between stations are as large as 70° for the diurnal constituents. These differences are as large as 120° for the semidiurnal constituents.

4) Although the amplitude of the overtide constituents is small (of the same order as the resolution of the instruments), both the amplitude and phase of these constituents is consistent and well defined.

5) Comparing the amplitudes and phases of the principal constituents at Stations 1, 2 and 20, it is clear that the northwest opening to the Bight is relatively opaque to the tides.

6) The K1 and S2 constituents are the only significant constituents in the atmospheric pressure rec-

ords. The instability in the amplitude and phase of the K1 constituent suggests that this constituent is probably a false contribution of S1 periodicity.

From the harmonic analysis of the atmospheric pressure records, a set of mean complex tidal amplitudes were computed. These were subtracted from the complex amplitudes of the bottom-mounted tide gage records to provide corrected estimates of the amplitude and phase of the seven tidal constituents. These are summarized graphically in Figs. 4, 5 and 6. Only data yielding relatively stable estimates are included in these figures. The resulting amplitude and phase distributions constitute the input for the model calculations in Part II of this series, and for the comparison of this model with experiment. We note the following features:

1) All constituents exhibit a minimum amplitude in the central part of the Bight.

2) The overtide constituents have maximum amplitude in the east to southeast part of the Bight.

3) The amplitude of the overtide constituents is

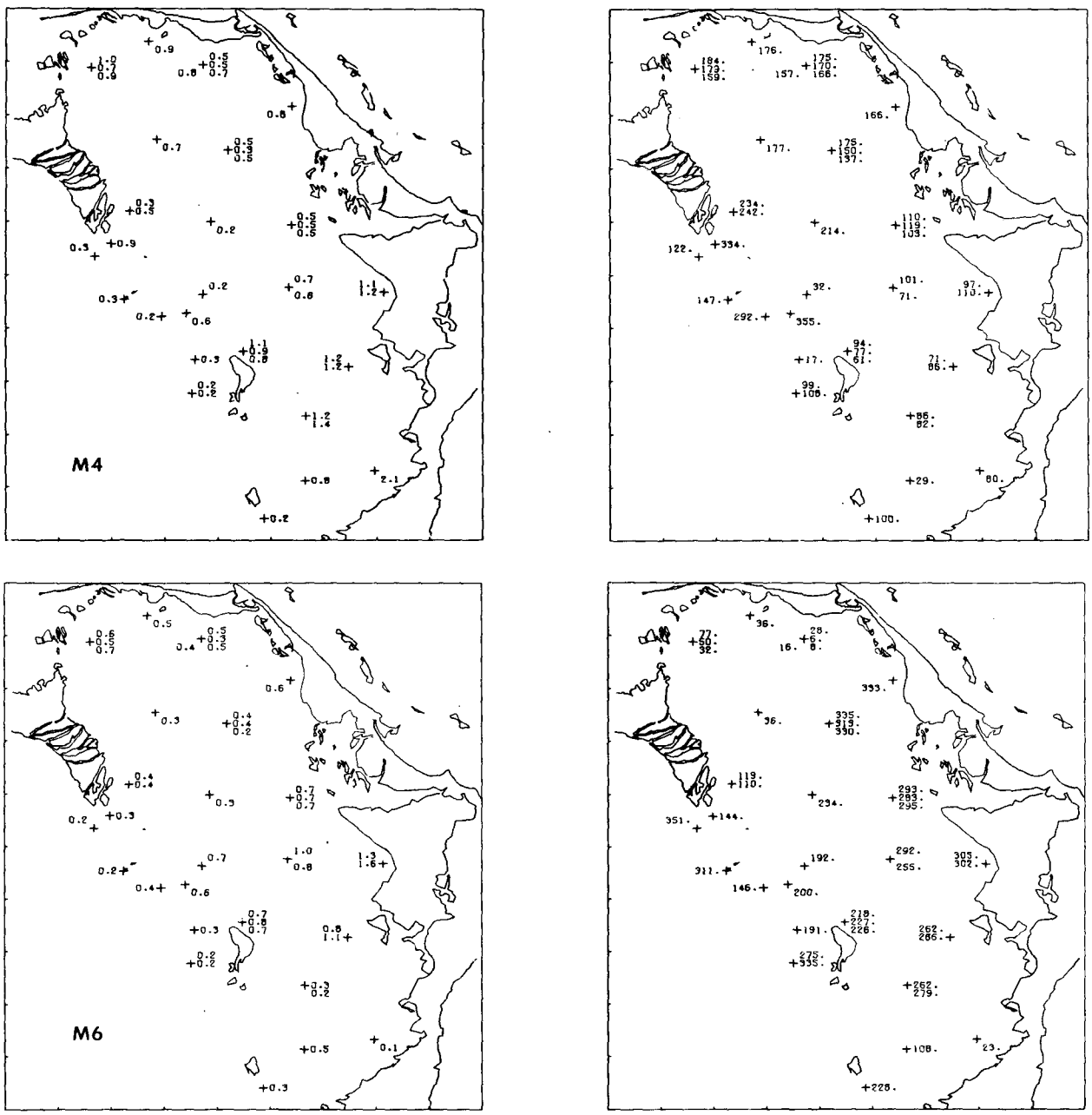

FIG. 6. As in Fig. 4 except for the overtide constituents M4 and M6.

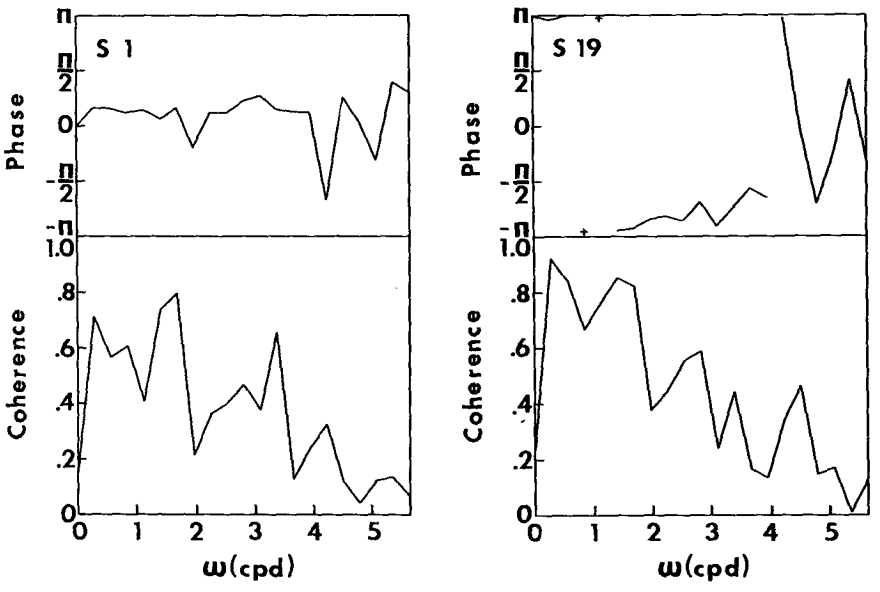

FIG. 7. Coherence and phase between the tidal residual and the north-northwest component of wind stress for Stations 1 and 19. Coherence is square coherence. Spectral estimates have 40 degrees of freedom.

small along the western margin of the Bight. (In Part II it will be assumed to vanish along this margin.)

4. Residual fluctuations

An estimate of the residual fluctuation ζ_R was computed from

$$\zeta_R' \equiv \zeta - \sum_{n=1}^{2N} {}_n\zeta_I' I_n$$

$$= \zeta_R + \sum_{n=2N+1}^{\infty} {}_n\zeta_I I_n - \sum_{n=1}^{2N} \Big[\sum_{l=2N+1}^{\infty} {}_nE_{I\ l}\zeta_I + \sum_{l=1}^{2N} {}_{nl}S_I^{-1}(I_l,\zeta_R) \Big] I_n.$$

The second term on the right represents a residual tidal fluctuation not included in the least-squares analysis. The remaining terms are the errors resulting from false contributions to the estimated tide from this residual tidal fluctuation and from the residual fluctuation ζ_R. The estimated residuals for the BOA data are shown in the Appendix. Inspection of these figures indicates that 1) the residuals are highly coherent; 2) the residuals for the February–March 1969 experiment are considerably more energetic than are those for the two summer experiments; and 3) the residuals contain appreciable tidal energy. In several instances, the tidal fluctuation dominates the record (typically stations along the western margin of the Bight). Further inspection of these figures indicates that 4) significant differential setup effects are present.

Fig. 7 shows the coherence and phase between the residuals for a pair of tide gages located at opposite ends of the Bight (Station 1 and 19), and the north-northwest (travel toward) component of wind stress at Station 11 during February–March 1969. Note that the Station 1 residual is in phase with and the Station 19 residual is out of phase with this stress, consistent with a differential setup to the north-northwest.

5. Conclusions

1) A relatively dense array of tide gages and weather stations has been used to acquire a detailed description of the tides and setup in a shallow, semi-enclosed basin, the Bight of Abaco, Bahamas.

2) The tides of this region exhibit a number of features which suggest that the frictional interaction inside the Bight is a significant factor in the tidal dynamics: (i) the amplitude of the principal constituents is significantly reduced inside the Bight relative to the western margin; (ii) measurable overtides (in particular, M6) are present and exhibit a relatively small amplitude along the western margin. This feature suggests that the overtides are generated locally and are contained within the region by reflection along the western margin (as a result of the depth discontinuity). It will be seen in Part II of this series (Snyder, *et al.*, 1979) that these features cannot be faithfully modeled with a quadratic friction law without either substantially modifying this law or allowing for significant nontidal flow.

3) Significant setup effects are present and are well correlated with the meteorology.

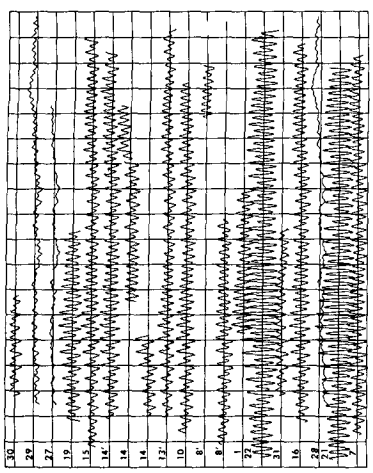

FIG. AIII(I)

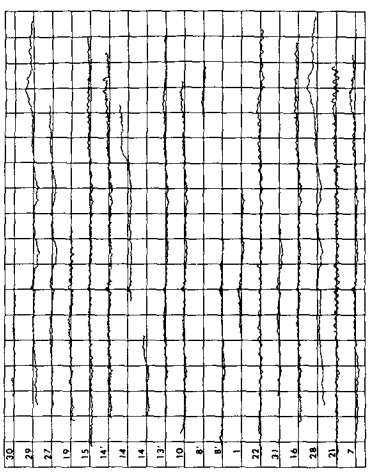

FIG. AIII(II)

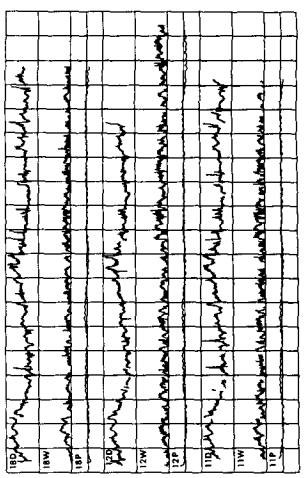

FIG. AIII(III)

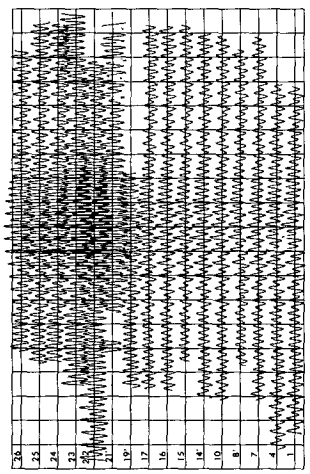

FIG. AII(I)

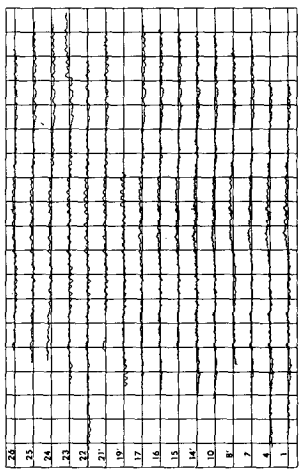

FIG. AII(II)

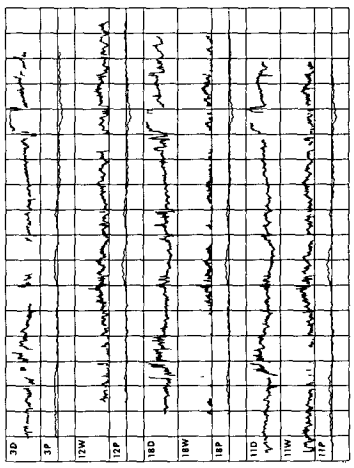

FIG. AII(III)

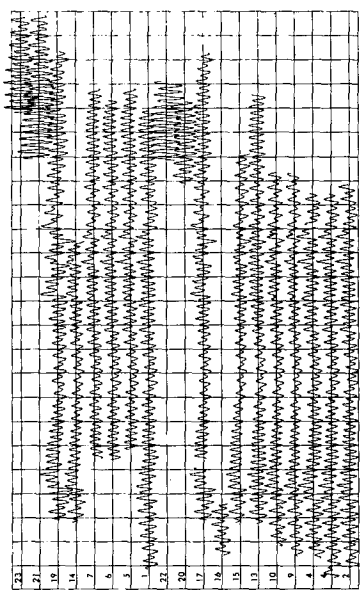

FIG. AI(I)

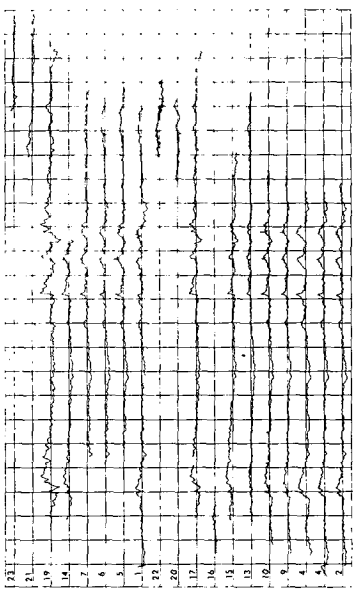

FIG. AI(II)

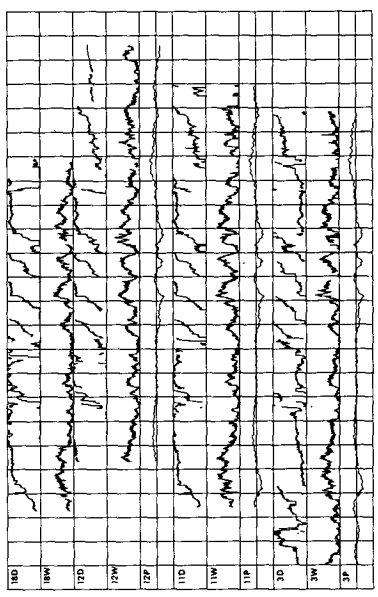

FIG. AI(III)

4) A generalization/hybridization of the algorithm of Munk and Hasselmann (1964) provides a convenient estimate for the errors of the tidal harmonic analysis.

5) High-quality synoptic geophysical data can be acquired economically using small research vessels.

Acknowledgments. Data for this study were collected from the vessels R/V *Gulf Stream* and R/V *L.F.R. Bellows*. We thank Captains Frank Davis and William Campbell for their cooperation and able boat handling. We thank Alan Carr for maintaining the Decca Hi-Fix; Linda Smith, Kathi Redmond and Odette Filloux for their help with the data reduction and analysis; and William Richardson for making available various facilities despite obvious conflicts with his research program. Finally, we thank David Hunley, Peter Niiler, Dennis Moore, Georges Weatherly, David Parrish and Alex Brincko for helping with the field experiments.

We are grateful to the Bahama authorities for allowing the Bight of Abaco to be used for the experiments. Financial support has been provided by National Science Foundation Grants GA-27352 and OCE 76-10739.

APPENDIX

Experimental Data

Tide data, estimated residuals and weather station data for the (AI) February–March 1969, (AII) July–August 1969 and (AIII) July–August 1970 experiments. Vertical bars are at 2-day increments beginning 0000 GMT 8 February 1969, 0000 GMT 10 July 1969 and 0000 GMT 9 July 1970, respectively.

Vertical scale for the tide data and for the residuals is 60 cm per division. Station 4 is a reed switch tide gage (upper trace, February–March 1969 experiment); remaining traces are bottom-mounted tide gages (uncorrected for atmospheric pressure).

Vertical scale for the weather station pressure records (P) is 60 cm (sea water) per full division; vertical scale for the wind speed records (W) runs from 0 to 20 m s^{-1}; vertical scale for the wind direction records (D) runs from 0° to 360° (angle of approach clockwise from north). During the February–March 1969 experiment, an offset is apparent between record 3D and the other direction records; this offset probably resulted from an error in the field calibration of the 3D vane.

REFERENCES

Baker, D. J., R. B. Wearn and W. Hill, 1973. Pressure and temperature measurements of the bottom of the Sargasso Sea. *Nature*, **245**, 25–26.

Filloux, J. H., 1970. Deep sea tide gages with optical readout of Bourdon tube rotations. *Nature*, **226**, 935–937.

——, 1973: Tidal patterns and energy balance in the Gulf of California. *Nature*, **243**, 217–221.

Munk, W. H., and K. Hasselmann, 1964: Super resolution of tides. *Studies in Oceanography*, University of Washington Press, 339–344.

Snodgrass, F. E., 1968: Deep sea instrument capsule. *Science*, **162**, 78–87.

Snyder, R. L., M. Sidjabat and J. H. Filloux, 1979: A study of tides, setup, and bottom friction in a shallow semi-enclosed basin. Part II. Tidal model and comparison with experiment. *J. Phys. Oceanogr.*, **9**, 170–188.